J. Fluid Mech. (1995), *vol.* 289, *pp.* 29–50

On the alignment and axisymmetrization of a vertically tilted geostrophic vortex

By F. VIERA

The School of Mathematics and Statistics, The University of Sydney, NSW, 2006, Australia

(Received 14 January 1994 and in revised form 13 October 1994)

We investigate the evolution of a vertically tilted geostrophic vortex of cylindrical shape and circular horizontal cross-section using the recently developed method of *boundary surface dynamics*. The vortex consists of a finite volume of constant potential vorticity immersed in a spatially unbounded fluid of uniform density stratification. The fully nonlinear three-dimensional problem is then reduced to the calculation of the Lagrangian evolution of the boundary surface of the vortex region, thus decreasing the dimensionality by one. In the numerical simulations presented here, the vortex shows a general tendency to attain vertical alignment and a horizontal axisymmetrical shape by wobbling about its centre and going through three basic stages of evolution: (*a*) the circular horizontal cross-sections of the upper and lower parts of the vortex distort and become elongated; (*b*) the upper and lower sections then become vertically aligned by reducing their horizontal intercentroid distances; and (*c*) the distorted horizontal cross-sections relax towards axisymmetry, often through the process of filamentation. For a given vortex height, if the horizontal scale of the flow is close to the internal radius of deformation, or equivalently, the density stratification is not too strong, the processes of filamentation and vertical alignment are enhanced. However, for stronger stratifications, both filamentation and vertical alignment are found to be greatly inhibited. For relatively small initial inclination angles, filamentation only occurs in the upper and lower sections of the vortex. Increasing the angle of tilt also increases the tendency of the surface to steepen and filament in the middle sections of the vortex. For a fixed value of the ratio of horizontal scale of the flow to the deformation radius, taller vortices have an increased tendency to align and axisymmetrize than shorter vortices of equal inclination angle.

1. Introduction

Strong isolated coherent structures play a fundamental role in the evolution of high Reynolds number turbulent flows. Numerical experiments of two-dimensional Eulerian flows by McWilliams (1984, 1990, and references therein), have shown that coherent vortices develop from random distributions of vorticity and eventually dominate the dynamics of the flow. The vortices appear spontaneously through relaxation towards axisymmetry of an isolated vorticity patch with a dominant sign in the vorticity field. Hence a clear understanding of the conditions leading to axisymmetrization is of paramount importance in the study of turbulent behaviour. This process has been studied in some detail by Melander, McWilliams & Zabusky (1987) who showed that in Eulerian and barotropic geostrophic flows, a near elliptical vortex evolves to axisymmetry as a result of an inviscid mechanism involving filamentation. In the case of two-layer stratified geostrophic flows, simulations of vortex interactions show that under certain conditions, vortex patches in different layers coalesce and become aligned

in the vertical direction by reducing their intercentroid separation. The new combined vortex then relaxes to a horizontal axisymmetrical shape through the processes of filamentation (Polvani 1991; Polvani, Zabusky & Flierl 1989).

In a continuously stratified fluid, high-resolution simulations of fully three-dimensional geostrophic turbulence by McWilliams (1989), showed that coherent vortices also emerge from random initial conditions where the vorticity is predominantly of a single sign. McWilliams provides a qualitative description of the role of vertical alignment and axisymmetrization in vortex formation, and clearly indicates the importance of these processes in the emergence and further evolution of a population of vortices in geostrophic turbulence. Rhines (1977, 1979), referred to these processes as the 'growth of barotropy' or 'barotropization' in cases with top and bottom boundaries present. In that case, there is a pattern of conversion of potential energy to kinetic energy and horizontal distortion of the potential vorticity contours that corresponds to the enstrophy cascade.

However, partly owing to the high costs involved in fully three-dimensional computations, the details of the processes of vortex formation in continuously stratified fluids are not well known. Viera (1994*b*) used the recently developed method of *boundary surface dynamics* (hereinafter BSD), to study the axisymmetrization from horizontal distortion of an elliptical right cylinder vortex of finite height embedded in a spatially unbounded, continuously stratified geostrophic fluid. Preliminary results showed that axisymmetrization was enhanced for horizontal scales L greater than the internal radius of deformation L_D with little or no filamentation, provided the aspect ratio of the elliptical cross-section is not too large. If the aspect ratio is large, horizontal fragmentation of the vortex occurs, and the outer levels (the top and bottom sections) split into two smaller vortices. On the other hand, we found that relaxation towards axisymmetry was inhibited for scales L smaller than L_D, that is, for relatively strong density stratification. In another related study, Viera (1994*c*) has shown that when two identical vertically offset cylindrical vortices interact with one another under certain conditions, they tend to align themselves by becoming vertically tilted in the initial stages of the evolution. For horizontal scales greater than L_D, the horizontal intercentroid separation of the top and bottom levels of the new tilted structure increased by as much as two or three times the initial vortex radius, depending upon the original configuration of the system. Some natural questions arise. Is the long time evolution of the resulting tilted structure a stable or unstable configuration? In other words, does the structure eventually reach a stable (possibly axisymmetric) shape or does it collapse due to vertical and/or horizontal fragmentation? Are there any conditions when alignment and axisymmetrization without filamentation are possible as in the case of Viera (1994*b*), or does it always filament in the process? If it does filament, what is the extent of filamentation? Does the value of the initial angle of inclination affect the rates of alignment and axisymmetrization?

In an attempt to obtain some insight into the problems posed by these questions, in this article we study the evolution of a cylindrical geostrophic vortex of finite height that is initially vertically tilted. The aim is to shed some light on the nature of the alignment and axisymmetrization processes that occur in a volume of fluid with a single sign in the vorticity field, as may appear in simulations of geostrophic turbulence. We assume a vortex of constant potential vorticity distribution in the horizontal direction, immersed in a spatially unbounded fluid of uniform stratification. We then apply the BSD method to reduce the fully nonlinear three-dimensional problem to the Lagrangian evolution of the two-dimensional boundary surface of the vortex region, thus decreasing the amount of computational effort involved. One of the advantages

of a Lagrangian algorithm such a BSD is the ability to capture the distortion of the material surfaces in great detail with only a moderate number of computations. Another characteristic of BSD is the capacity to describe continuously stratified geostrophic flows without the necessary introduction of a layered structure in the vertical direction. The governing equations are first transformed into integrals over the vortex surface and then discretized directly to compute the velocity field of the flow. An immediate consequence of the fully three-dimensional approach is that the singular integrals that normally appear in the numerical discretizations are easily desingularized using a straightforward change of variables, yielding a simple and robust algorithm.

The principal aim of the paper is to present preliminary investigations obtained from numerical experiments using BSD, to help identify general qualitative conditions that may enhance or inhibit the process of evolution towards a vertically aligned axisymmetric configuration. The organization of the article is as follows. In §2 we introduce the governing equations and give a brief overview of the BSD equations and numerical algorithm. In §3 we elaborate on the concepts of vortex alignment and axisymmetrization and present simulations for several values of the model parameters such as the tilt angle and the stratification strength. Finally, in §4 we give a summary and discussion and outline some outstanding problems requiring further investigation.

2. The BSD algorithm

The quasi-geostrophic potential vorticity in large-scale rapidly rotating continuously stratified flows in the oceans and planetary atmospheres is conserved following fluid particles of horizontal velocity (u, v). That is,

$$\frac{\partial Q}{\partial t}+u\frac{\partial Q}{\partial x}+v\frac{\partial Q}{\partial y}=0, \tag{1}$$

where the potential vorticity is

$$Q(x,y,z)=\frac{\partial^2\psi}{\partial x^2}+\frac{\partial^2\psi}{\partial y^2}+\frac{1}{\gamma^2}\frac{\partial^2\psi}{\partial z^2}, \tag{2}$$

and where $\psi(x, y, z, t)$ is the stream function such that $(u, v) = (-\psi_y, \psi_x)$. The strength of the stratification is measured by

$$\gamma=\frac{L_D}{L},\quad L_D=\frac{\mathcal{N}D}{f},\quad \mathcal{N}=\left\{\frac{-g}{\rho}\frac{\partial\rho}{\partial z}\right\}^{1/2}, \tag{3}$$

where L_D is the internal radius of deformation of the fluid, $\mathcal{N}$ is the uniform Brunt–Väisälä frequency, f is the spatially uniform Coriolis parameter, $\rho(z)$ the density and L, D are characteristic horizontal and vertical lengthscales respectively. The equations are valid when the Rossby number $R_0 = U/fL \ll 1$, where U is a characteristic velocity scale of the flow. This condition is satisfied for large-scale flows where rotation is important. See for example Pedlosky (1979) for a derivation and conditions of validity of (1)–(3), and Charney (1963), who first discussed the extension of the concept of point vortices to a continuously stratified quasi-geostrophic fluid.

To apply the BSD method we assume a vortex consisting of a finite volume V in a spatially unbounded fluid such that the potential vorticity

$$Q(x,y,z)=\begin{cases}Q_I(z) & \text{inside } V\\ Q_O(z) & \text{outside } V,\end{cases} \tag{4}$$

where Q_I and Q_O are functions of z only, i.e. the potential vorticity field is piecewise-constant horizontally, but can have an arbitrary variation in the vertical direction. Then it can be shown (Viera 1994*a*) that the velocity field may be written in the integral form

$$(u,v) = -\frac{1}{4\pi}\iint_S \Delta Q(z')\, G(\boldsymbol{r},\boldsymbol{r}')\,(\mathrm{d}x',\mathrm{d}y')\,\mathrm{d}z', \tag{5}$$

where S is the closed surface enclosing the volume V,

$$\Delta Q(z') = Q_O(z') - Q_I(z') \tag{6}$$

is the potential vorticity difference between outside and inside the vortex, and

$$G(\boldsymbol{r},\boldsymbol{r}') = \gamma[(x-x')^2+(y-y')^2+\gamma^2(z-z')^2]^{-1/2} \tag{7}$$

is the Green's function of the Laplace operator on the right-hand side of (2). Since potential vorticity is conserved following fluid particles of horizontal velocity (u,v), the problem is completely determined by following the evolution of the material boundary surface S using the Lagrangian equations

$$\frac{\mathrm{d}x}{\mathrm{d}t} = u(x,y,z,t), \quad \frac{\mathrm{d}y}{\mathrm{d}t} = v(x,y,z,t), \tag{8}$$

where the velocity field is evaluated at the surface S. The three-dimensional problem has been reduced to the evolution of the two-dimensional boundary surface of the vortex region V. Equations (5)–(8) are the boundary surface dynamic equations describing the fully nonlinear three-dimensional evolution of geostrophic vortices in a continuously stratified fluid.

The numerical algorithm is implemented by writing (5) in the form

$$(u,v) = -\frac{1}{4\pi}\int_{z_B}^{z_T} \Delta Q(z')\, M^{(u,v)}(z')\,\mathrm{d}z', \tag{9a}$$

where

$$M^{(u,v)}(z') = \oint_{\mathscr{C}} G(\boldsymbol{r},\boldsymbol{r}')\,(\mathrm{d}x',\mathrm{d}y'), \tag{9b}$$

$\mathscr{C}$ is a closed curve obtained by the intersection of S with a horizontal plane $z = z_k$ ($z_B \leqslant z_k \leqslant z_T$), and z_B and z_T are the bottom and top levels of the vortex respectively. (The word *level* is used in this context simply as a convenient way to specify a horizontal cross-section of the vortex at a given value of z in the spatial discretizations. It has no relation to the so-called *level-models* used elsewhere in the literature.) The superscripts (u,v) refer to the (x',y')-integrals of the (u,v)-components of the velocity field respectively. The surface S is discretized by a set of points (x_{ik}, y_{ik}, z_k) such that $0 \leqslant i \leqslant N+1$ and $1 \leqslant k \leqslant N_z$, where N_z is the number of z-levels, $N+2$ the number of points on each level and $z_B \equiv z_1$ and $z_T \equiv z_{N_z}$.

Using the trapezoidal rule gives

$$M^{(u)}(z_l) = \tfrac{1}{2}(x_{1l}-x_{Nl})\,M_{0l} + \tfrac{1}{2}\sum_{j=1}^{N}(x_{j+1l}-x_{j-1l})\,M_{jl}, \tag{10a}$$

$$M^{(v)}(z_l) = \tfrac{1}{2}(y_{1l}-y_{Nl})\,M_{0l} + \tfrac{1}{2}\sum_{j=1}^{N}(y_{j+1l}-y_{j-1l})\,M_{jl}, \tag{10b}$$

where

$$M_{jl} = \begin{cases} G(R_{jl}) & \text{for} \quad (j,l) \neq (i,k) \\ 0 & \text{for} \quad (j,l) = (i,k), \end{cases} \tag{11a}$$

and

$$G(R_{jl}) = \gamma[(x_{ik}-x_{jl})^2+(y_{ik}-y_{jl})^2+\gamma^2(z_k-z_l)^2]^{-1/2}. \tag{11b}$$

To close the contour we have taken $(x_{0k}, y_{0k}) = (x_{N+1k}, y_{N+1k})$ in (10*a*, *b*). Next, using Simpson's rule quadrature in the z-direction with N_z odd, the velocity field becomes

$$(u_{ik}, v_{ik}) = -\frac{1}{4\pi}\left\{\frac{\Delta z}{3}\left[M^{(u,v)}(z_1)\ \Delta Q(z_1) + M^{(u,v)}(z_{N_z})\Delta Q(z_{N_z}) + 4\sum_{\substack{l=2\\ l\,\text{even}}}^{N_z-1} M^{(u,v)}(z_l)\,\Delta Q(z_l) + 2\sum_{\substack{l=3\\ l\,\text{odd}}}^{N_z-2} M^{(u,v)}(z_l)\,\Delta Q(z_l)\right] + I_{ik}^{(u,v)}\right\}. \tag{12}$$

The expressions $I_{ik}^{(u,v)}$ are singular integrals over a small surface patch containing the singular point (x_{ik}, y_{ik}, z_k) (see Viera 1994*a* for details of desingularization and computation of the integrals I_{ik}). The time stepping is performed using a standard fourth-order Runge–Kutta method. To maintain an adequate resolution for longer integration times and increase computational efficiency, a node insertion/deletion scheme is included in each level. A node is inserted between two consecutive points if their distance $d_i > \epsilon$ where

$$\epsilon = \max\left[\min\left(0.1\kappa^{-1}, S_{max}\right), 0.021\right], \quad S_{max} = \min\left[0.03P, 0.15\right],$$

κ is the local contour curvature, and P the perimeter of the contour. A node is deleted if $d_i < \max[0.02, 0.1\epsilon]$. These parameters were obtained by numerical experimentation and found suitable for the present application.

3. Numerical simulations

The initial condition consists of a tilted cylindrical vortex of circular horizontal cross-section of unit radius, with a horizontal intercentroid distance D_i between the bottom and top levels z_B and z_T, as shown in figure 1 at $t = 0$. The vortex height is V_h and we set $z_B = -V_h, z_T = 0$ and the vortex centre at the point $(x, y, z) = (0, 0, -\frac{1}{2}V_h)$. Although BSD does not require a constant potential vorticity distribution in the vertical, in order to keep the number of free parameters to a minimum, a constant potential vorticity is assumed in the vertical direction also. We note from (5) and (8) that if ΔQ is independent of z, then $|\Delta Q|$ can be absorbed into the timescale. Hence, without loss of generality, we set $Q_I = 1$ and $Q_O = 0$, giving $\Delta Q = -1$. Thus, we are left with two independent parameters in the system. One is the angle of tilt θ_i, where $\tan\theta_i = D_i/V_h$. Another convenient parameter in the present simulations is γ/V_h, what might be termed an 'effective' stratification strength. It takes into account the effects of stratification changes, directly from changes in the Brunt–Väisälä frequency $\mathcal{N}$ and indirectly from changes in the vortex height. This can be easily seen from the definition of γ in (3), where we note that increasing (decreasing) the vertical lengthscale D is equivalent to decreasing (increasing) $\mathcal{N}$, for a fixed value of γ. In other words, tall vortices in a strongly stratified fluid have a similar behaviour to shorter vortices in a weaker stratified environment. In all simulations we take $N_z = 29$ and a time step $\Delta t = 0.4$, except in Run 5, where a higher resolution of $N_z = 61$ is used. The initial number of nodes on each horizontal level is $N = 70$ and this number is allowed to increase to a maximum of about 350 points depending on the complexity of the flow. Since potential vorticity is conserved, the vortex volume remains constant throughout the evolution. This fact was used to check the accuracy of the calculations and it was found that although the vortex experienced large deformations in some cases, the volume change remained less than 0.5% at the end of each run.

Since the advecting velocity in the quasi-geostrophic equation (1) involves only the horizontal part of the velocity field, the fluid particles comprising the boundary of a

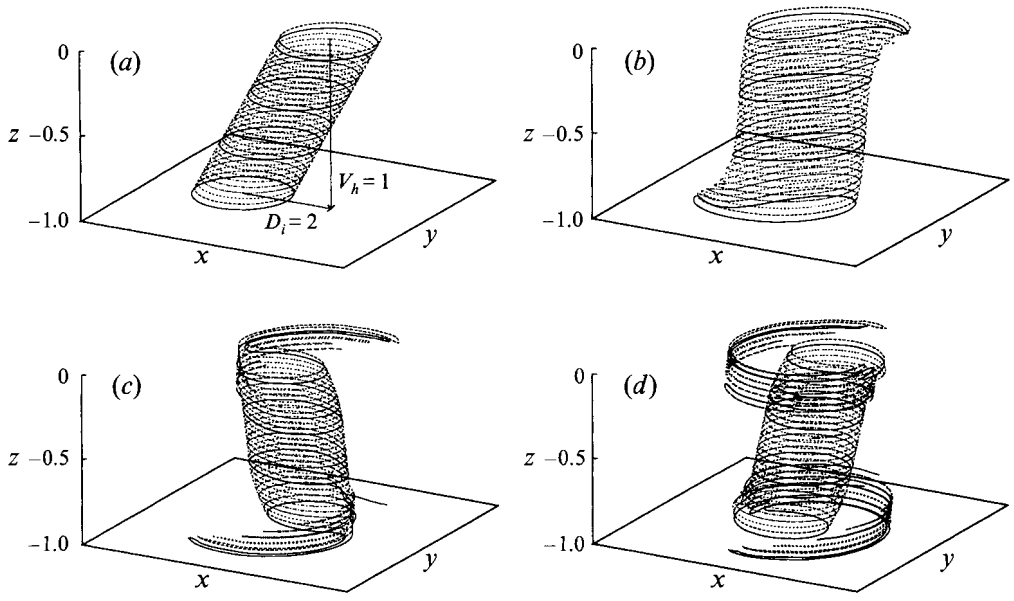

FIGURE 1. Three-dimensional view of the vortex evolution for $D_i/V_h = 2$, $\gamma/V_h = 1$, $N_z = 29$ and $\Delta z = 0.0357$ (Run 1): (*a*) $t = 0$, (*b*) $t = 20$, (*c*) $t = 40$, (*d*) $t = 60$.

Run	D_i	V_h	γ	D_i/V_h	γ/V_h	N_z	Figures
1	2	1	1	2	1	29	1–5
2	4	1	1	4	1	29	6–10
3	1	0.5	1	2	2	29	11–14
4	2	1	3	2	3	29	15–18
5	4	2	1	2	0.5	61	19–24

TABLE 1. The parameters used in the five simulations and their corresponding figure numbers. There are only two independent parameters in the system, and we have chosen the tilt angle, given by $\tan\theta_i = D_i/V_h$, and an 'effective' stratification strength given by γ/V_h.

given horizontal cross-section will remain at the same vertical level throughout the evolution. Hence, for the purpose of discussing the results of the simulations in the present context, it will be convenient to refer to the vortex evolution as consisting of the following two main components, as discussed by McWilliams (1989): (*a*) *vertical alignment* of the different sections of the vortex, defined as the extent to which the vortex axis (i.e. the line joining the centroids of all the horizontal cross-sections) becomes close to a vertical straight line; (*b*) *horizontal axisymmetrization*, which is the extent to which the boundaries of a horizontal cross-section at a given level reach a circular shape. The latter appears in a two-dimensional fluid, as we mentioned in §1, and can be interpreted in terms of fluid trajectories of the conserved potential vorticity. The former, on the other hand, requires the third dimension and has more fundamentally the character of action-at-a-distance since information is conveyed vertically only through the Green's function relating potential vorticity to the motion. Our aim here will be to determine to what degree these two conditions are satisfied at the end of the evolution.

We ran a total of five simulations whose parameter values are shown in table 1. In the first simulation (Run 1) we let $\gamma = 1$, $V_h = 1$ and $D_i = 2$. These values correspond

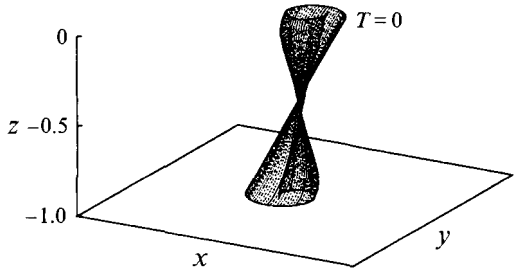

FIGURE 2. The evolution of the vortex axis, defined as the line joining the centroids of all the horizontal cross-sections, for $D_t/V_h = 2$ (Run 1).

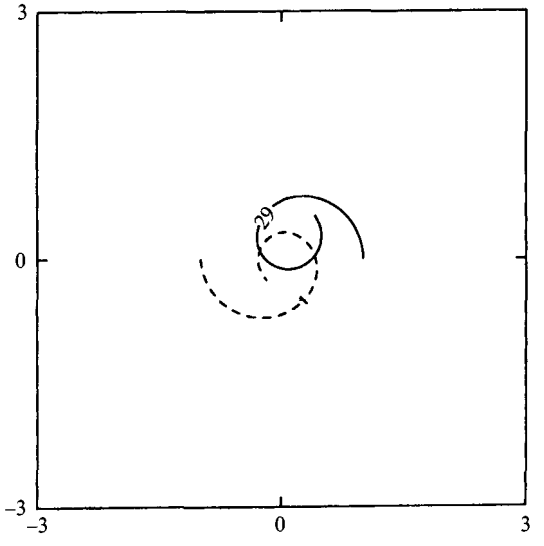

FIGURE 3. Trajectories of the centroids of the bottom and top levels 1 and 29, respectively, for $D_t/V_h = 2$ (Run 1).

to an inclination angle with the vertical of $\theta_i = \arctan 2 \approx 63°$ and a stratification strength $\gamma/V_h = 1$. We take $N_z = 29$ and hence $\Delta z = 0.0357$. Since the vortex is symmetric about its centre, we anticipate that its evolution will also be symmetrical about the centre. In particular, the centre itself will remain fixed throughout the evolution. However, we point out that owing to a slight asymmetry introduced by the numerical discretizations, the evolution will have a slight departure from perfect symmetry. Figure 1 shows the three-dimensional view of the vortex evolution at times $t = 0$, 20, 40 and 60, with the variable range in the horizontal plane being $-3 < x$, $y < 3$. One important feature of the evolution is the clear tendency of the vortex to wobble about its fixed centre while decreasing the inclination angle with the vertical in the process. This is confirmed by the plot of figure 2, which shows the three-dimensional trajectory of the cylinder axis (recall that the axis is the line joining the centroids of all the horizontal levels). It is clear that the middle sections of the vortex remain relatively fixed while the structure wobbles about its centre. The extent of the wobbling motion is seen in figure 3 where we plot the trajectories of the centroids of the bottom and top levels, 1 and 29 respectively. Their intercentroid distance decreases as the trajectories spiral inwards, showing the tendency of the levels to increase their vertical alignment.

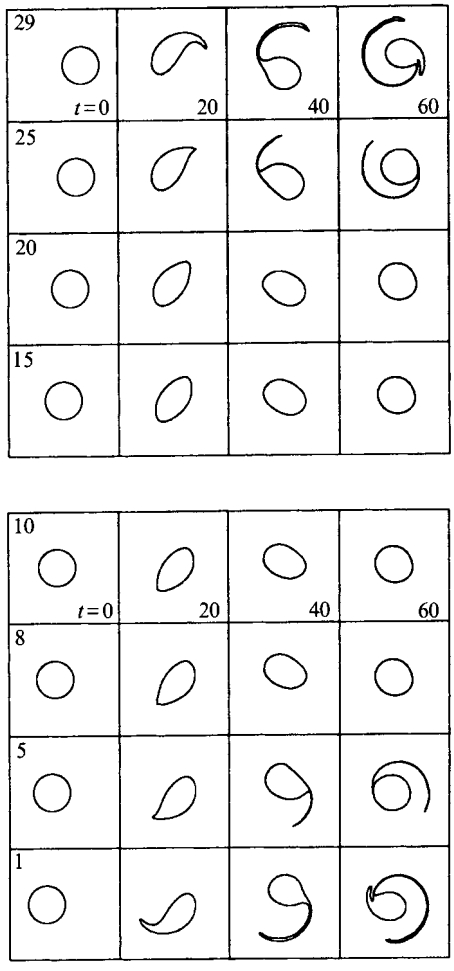

FIGURE 4. The evolution of the horizontal cross-sections of the vortex for $D_i/V_h = 2$ (Run 1). The number on the left-hand frames indicate the level k and time is shown from left to right. The vertical position of a level k is $z = \Delta z(k - N_z)$.

Another characteristic of the evolution of figure 1 is the large horizontal distortion of the structure observed at $t = 20$, followed by the formation of long filaments in the upper and lower sections at $t = 40$ and 60. In order to capture the details of the evolution of the horizontal cross-sections, eight selected levels are plotted in figure 4. Levels 1, 5, 8 and 10 correspond to the lower section while levels 15, 20, 25 and 29 correspond to the upper section. The level number k is shown in the top corner of the left-hand frames and time is given from left to right. The vertical position of a given level k can be found by calculating $z = \Delta z(k - N_z)$. The variable range of each frame is the same as that for figure 1 ($-3 < x, y < 3$). Since the evolution is symmetric about the vortex centre, the shape of level 29, for example, can be obtained by rotating level 1 through an angle π about the vertical line passing through the vortex centre. At $t = 20$, the shapes have become elongated and nonlinear steepening begins to appear at the boundaries of the outer levels 1, 5 and 25, 29. The wave disturbance in levels 1 and 29 is about to break, with breaking being defined here as the onset of filamentation. The inner levels 8 to 20 have an elongated oval shape and (with the exception of level 8) show no sign of steepening. At $t = 40$ the disturbance of the outer levels finally breaks

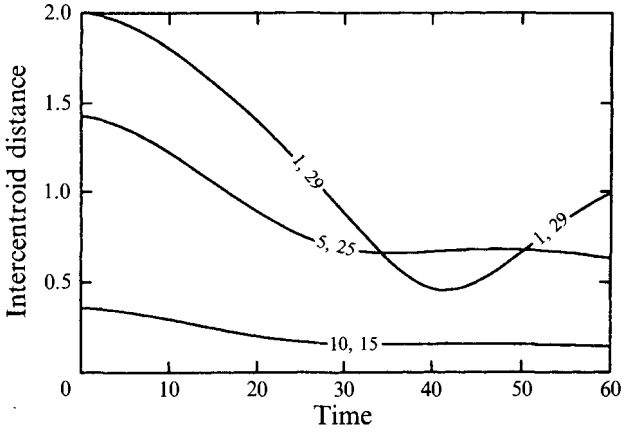

FIGURE 5. The intercentroid distance as a function of time, between the levels indicated by the numbers on the curves, for $D_i/V_h = 2$ (Run 1).

with the formation of a filament, and the horizontal boundaries show a tendency to return to an axisymmetrical shape. Levels 8 to 20 now have a more rounded oval shape and although level 8 showed a slight tendency to steepen at $t = 20$, the extent was not sufficiently large to allow breaking and subsequent filamentation to occur. The last column gives the evolution at $t = 60$. All levels attain a remarkably high degree of axisymmetry, despite the large distortion experienced in the initial stages. The inner levels 8, 10, 15 and 20 return to an almost circular shape without filamentation, while the outer levels retain a long thin filamentary tail attached to them. Levels 1 and 29 show the initial stages of what appears to be the formation of a secondary filament near where the original (primary) filament is about to detach.

It is clear that the horizontal distortion of the top and bottom sections of the vortex increases up to a point where the surface steepens, breaks and filaments. As we move away from the vortex centre towards the top or bottom levels, the filaments become longer and wider as is clearly seen in figure 1 at $t = 40$ and 60. In this case ($D_i = 2$), the first levels away from the centre to break and filaments are $z_7 \approx -0.79$ and $z_{23} \approx -0.21$. That is, the vertical distance from the centre where filamentation first occurs is $D_m \approx 0.29$. Levels further away than D_m on both sides of the centre return to axisymmetry through filamentation while those closer than D_m attain a nearly circular shape without sufficient steepening for filamentation to occur. Experiments run with smaller values of D_i (not shown here because of the similar qualitative behaviour), indicate that the distance D_m increases with decreasing D_i until filamentation is entirely absent from the vortex surface. This is not unexpected, since the vortex axis becomes almost vertical for small D_i, and therefore distortion and steepening of the surface are reduced, with consequent suppression of the filamentation process.

We now turn to the question of vertical alignment of the different sections of the vortex, as opposed to the axisymmetrization of the horizontal cross-sections. In order to obtain a quantitative measure of the degree of alignment, in figure 5 we plot the horizontal intercentroid distances $d_c(1, 29)$, $d_c(5, 25)$ and $d_c(10, 15)$ as a function of time (the notation $d_c(k_1, k_2)$ is used to denote the horizontal intercentroid separation between levels k_1 and k_2). One point is worth mentioning here. In the ideal case of a cylinder attaining the vertical position without distortion of the axis in the process, the curves would not cross one another and should intersect the *time*-axis simultaneously at a single point. Therefore, the behaviour of the intercentroid distance curves gives a

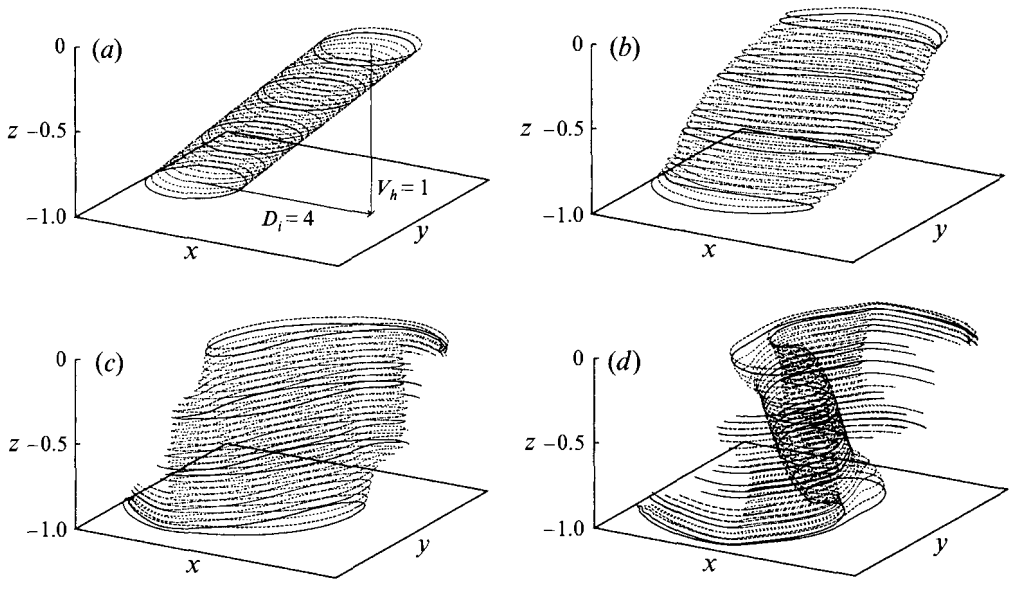

FIGURE 6. The vortex evolution for $D_i/V_h = 4$ and $\gamma/V_h = 1$ (Run 2): (*a*) $t = 0$, (*b*) $t = 20$, (*c*) $t = 40$, (*d*) $t = 60$.

qualitative indication of the extent of distortion of the vortex axis throughout the evolution. For example, the curve $d_c(1, 29)$ decreases from the initial value $D_i = 2$, to a value $D_f \approx 1$ at $t = 60$ after passing through a local minimum at about $t = 40$. The curve appears to behave in an oscillatory manner, twice intersecting the curve $d_c(5, 25)$ which decreases in a monotonic fashion. The curve $d_c(10, 15)$ also increases monotonically up to $t = 30$ and then remains almost constant thereafter. This indicates that the vortex axis experiences considerable distortion while attaining the upright position. This behaviour has also been observed in figure 2, where the cylinder axis is clearly curved in the upper and lower sections near the end of the evolution, compared to the straight line shape at $t = 0$. The fractional change of $d_c(1, 29)$ at the end of the run is

$$\Delta D = (D_i - D_f)/D_i \approx 50\%,$$

indicating that despite the fact that the curve is increasing at $t = 60$, the outer levels have achieved a relatively large degree of vertical alignment. The curve $d_c(1, 29)$ has negative concavity near the end of the run and shows a tendency to reach a maximum value soon after $t = 60$. However, simulations with extended time intervals would be required to determine its exact behaviour after that point.

Figure 6 shows the evolution for $D_i = 4$ (Run 2), with all other parameters as for figure 1. This corresponds to an angle of tilt $\theta_i = \arctan 4 \approx 76°$. An immediate consequence of the larger vertical tilting is the increased vertical distortion of the vortex in the earlier stages of evolution. The horizontal cross-sections given in figure 7 show the internal levels 8 to 20 with a more elongated shape at $t = 20$ and 40 compared to the corresponding shapes in figure 4 for $D_i = 2$. All levels now filament at $t = 60$. In particular, the middle level $z_{15} = -\frac{1}{2}$, whose shape is symmetric about the vortex centre, becomes quite elongated at $t = 40$ and breaks with the formation of two filaments at $t = 60$. All other levels near the centre have two filaments while those near the top and bottom sections finish up with only one long and relatively wide filament similar to those in figure 1 for $D_i = 2$. Hence, increasing the tilting angle has the effect of increasing the nonlinear steepening in the middle section of the vortex surface, with

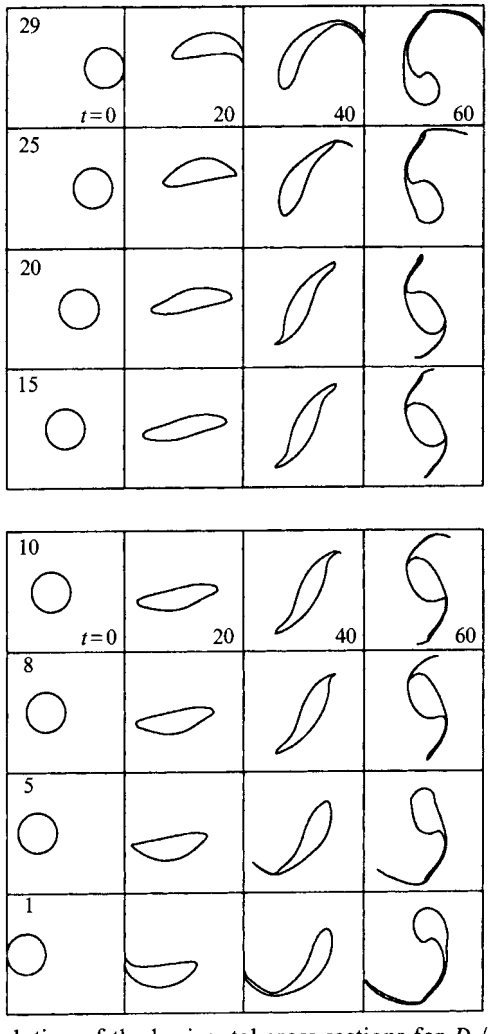

FIGURE 7. Evolution of the horizontal cross-sections for $D_t/V_h = 4$ (Run 2).

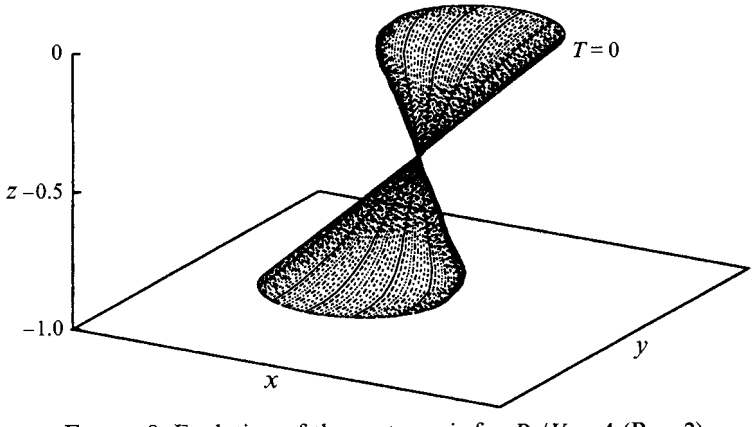

FIGURE 8. Evolution of the vortex axis for $D_t/V_h = 4$ (Run 2).

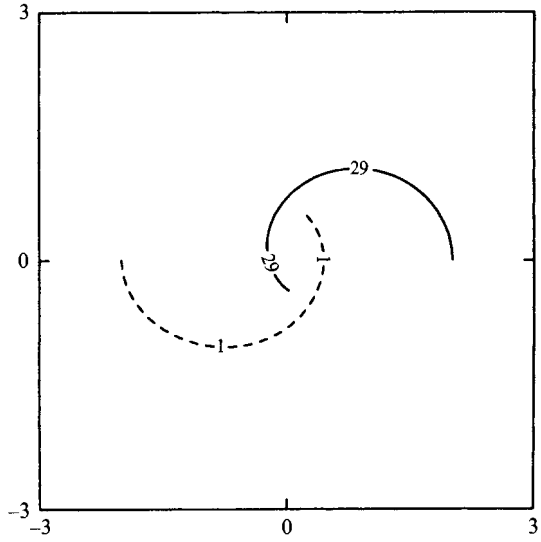

FIGURE 9. Trajectories of the centroids of levels 1 and 29 for $D_i/V_h = 4$ (Run 2).

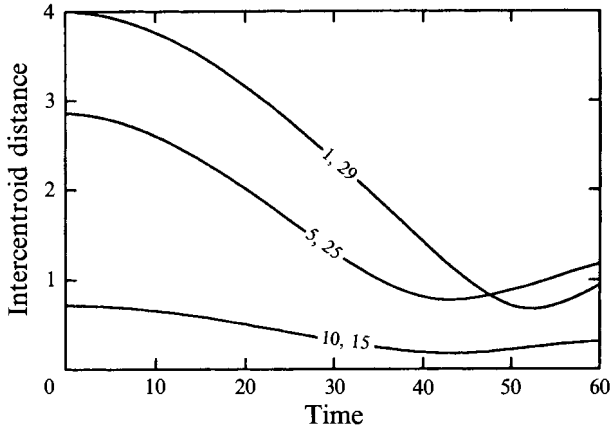

FIGURE 10. The intercentroid distances for $D_i/V_h = 4$ (Run 2).

consequent breaking and filamentation occurring in all levels of the structure. The curved shape of the axis at the end of the evolution in figure 8 indicates that the vortex undergoes a large amount of vertical distortion while attaining the upright position.

Another effect of a larger angle of tilt is an increase in the extent of wobbling motion of the vortex. This is shown by the open shape of the trajectories of the centroids of levels 1 and 29, plotted in figure 9. However, although the curves do not spiral inwards in this case, the final position of the centroids leads to an intercentroid separation of almost the same value as the case $D_i = 2$. This is confirmed by the plots of the intercentroid distances in figure 10. They show the alignment curve $d_c(1, 29)$ decreasing from the initial value $D_i = 4$ to a final value $D_f \approx 1$, which gives a fractional decrease at the end of the run of $\Delta D \approx 75\%$. This shows that alignment is larger at $t = 60$ than in the previous case. However, owing to the oscillatory nature of the curves, a more appropriate comparison of the extent of alignment in the early stages of the evolution is given by the average rates of decrease from $t = 0$ to the point where the first minimum occurs. They are given approximately by $1.5/40 \approx 0.04$ and $3.5/50 \approx 0.07$

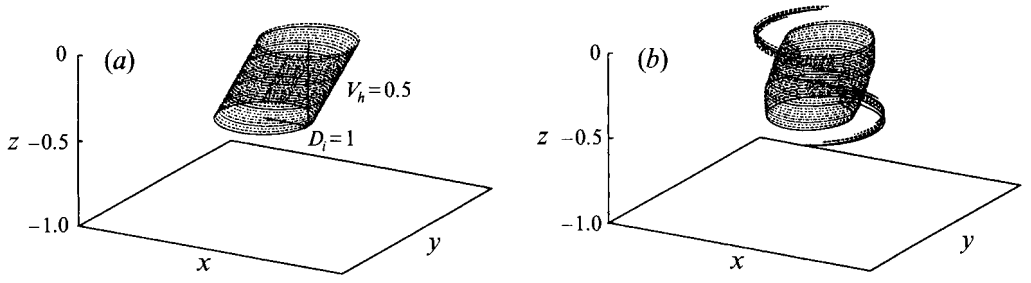

FIGURE 11. The vortex evolution at (*a*) $t = 0$, and (*b*) 60 for $D_i/V_h = 2$ and $\gamma/V_H = 2$ ($\gamma = 1$ and $V_h = 0.5$). (Run 3).

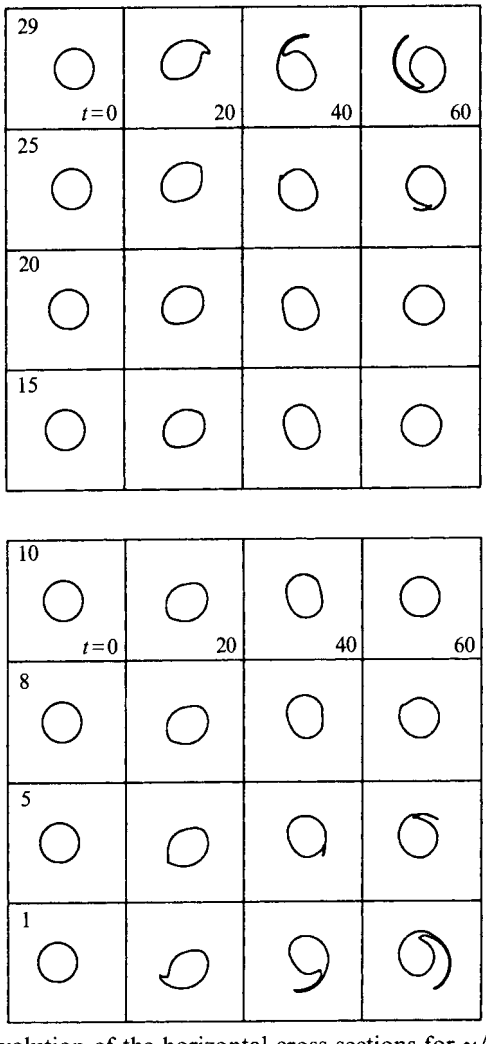

FIGURE 12. Evolution of the horizontal cross-sections for $\gamma/V_H = 2$ (Run 3).

for the curves $d_c(1, 29)$ in figures 5 and 10, respectively, and indicate that there is in fact an overall increase in the rate of alignment of the top and bottom levels 1 and 29 when the tilt angle is increased.

In the next set of simulations (Runs 3, 4 and 5), we return to a value of the tilt angle

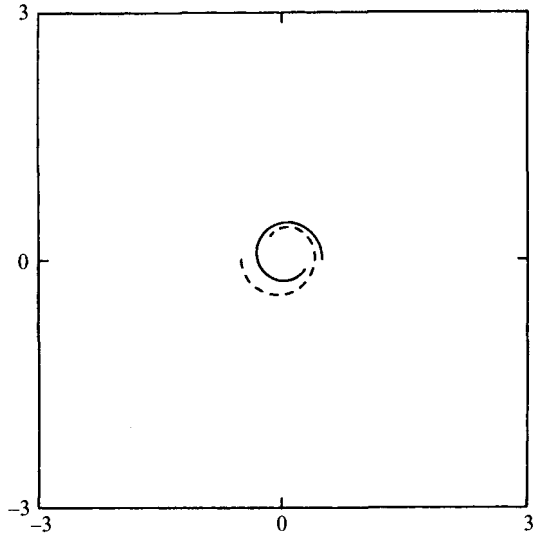

FIGURE 13. Trajectories of the centroids of levels 1 (dashed curve) and 29 (full curve) for $\gamma/V_H = 2$ (Run 3).

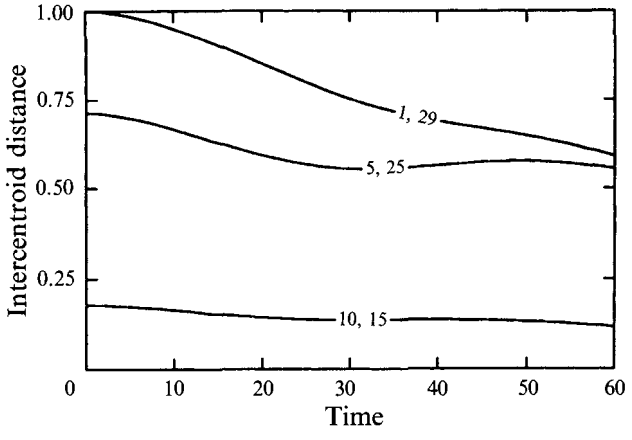

FIGURE 14. The intercentroid distances for $\gamma/V_H = 2$ (Run 3).

of $\tan\theta_i = D_i/V_h = 2$ and study the effects of varying the stratification strength γ/V_h. This is done in two different ways. In Runs 3 and 5 we change the vortex height V_h and fix $\gamma = 1$ and in Run 4 we set $V_h = 1$ and increase γ. The main reason for taking this approach is numerical convenience. It was found that, in the present simulations, small values of γ tend to produce a high-wavenumber instability in the filamentary bands near the end of the evolution. Although the main vortex core was unaffected, we found that using a value of $\gamma = 1$ and increasing V_h eliminates this problem and provides an alternative way to adjust the stratification strength. Figure 11 shows the evolution at $t = 0$, 60, for $\gamma/V_h = 2$ (Run 3). Here, the stratification is increased by decreasing the vortex height to $V_h = 0.5$ and keeping $\gamma = 1$. The main effect of a stronger stratification is to slow down the evolution and consequently decrease the length of the filaments ejected and the extent of vertical alignment. The evolution of the horizontal levels is shown in figure 12. Although the boundaries of the outer levels 1, 5 and 25, 29 steepen at $t = 20$, they have a more rounded, less elongated shape than the corresponding levels

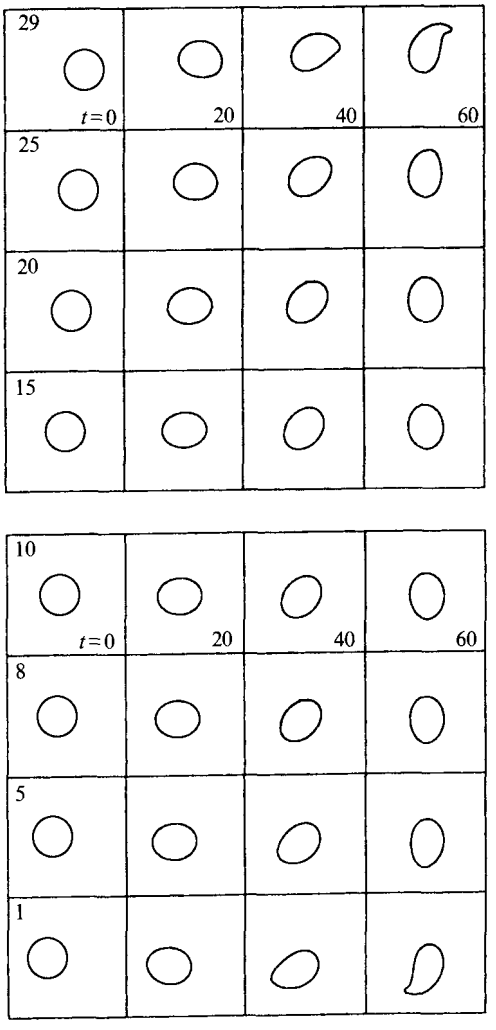

FIGURE 15. Evolution of the horizontal cross-sections for $D_t/V_h = 2$ and $\gamma/V_h = 3$ (Run 4).

for $\gamma/V_h = 1$ in figure 4. At $t = 40$ the outer levels filament while the inner levels 8 to 20 attain a slightly elongated oval shape. At $t = 60$ all levels return to an almost axisymmetrical shape, the inner levels doing so without filamenting in the process. The distances travelled by the centroids of the top and bottom levels 1 and 29 are shown in the plots of figure 13. The shorter path described in this case results in a relatively small reduction of the intercentroid separation between the two levels, as can be seen more clearly in figure 14. The curve $d_c(1, 29)$ decreases to $D_f \approx 0.6$, giving a fractional decrease of $\Delta D \approx 40\,\%$ at $t = 60$. The curves $d_c(5, 25)$ and $d_c(10, 15)$ decrease very slowly with the former exhibiting an oscillatory decay.

In the next simulation (Run 4), we increase the stratification even further to $\gamma/V_h = 3$ by taking $\gamma = 3$ and a vortex height $V_h = 1$. Figure 15 shows the evolution of the horizontal cross-sections. The extent of distortion has been further reduced compared to the previous run with $\gamma/V_h = 2$, and filamentation has not occurred at the end of the simulation. All levels show a slight tendency to elongate, but it is only at $t = 60$ that levels 1 and 29 show a more pronounced steepening of the boundary. The three-dimensional plots in figure 16 clearly indicate that only the four outer levels 1, 2 and

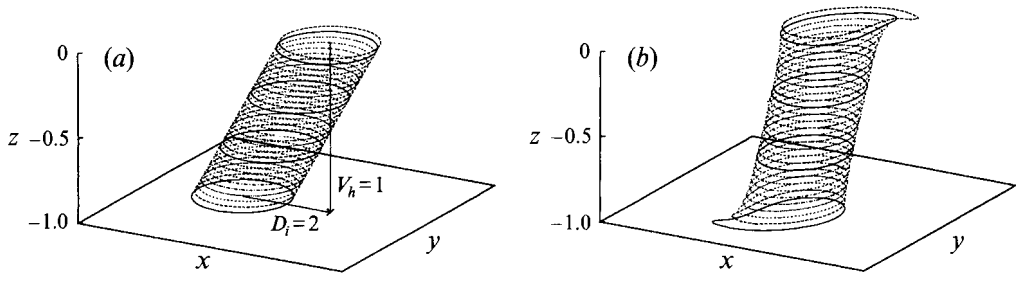

FIGURE 16. The vortex evolution at (*a*) $t = 0$ and (*b*) 60 for $\gamma/V_h = 3$ (Run 4).

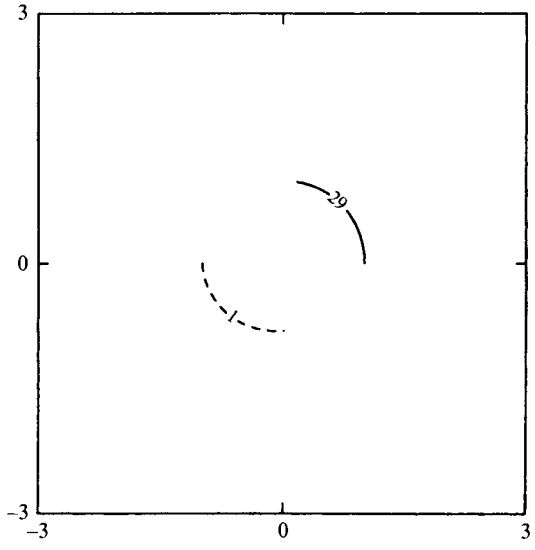

FIGURE 17. Trajectories of the centroids of levels 1 and 29 for $\gamma/V_h = 3$ (Run 4).

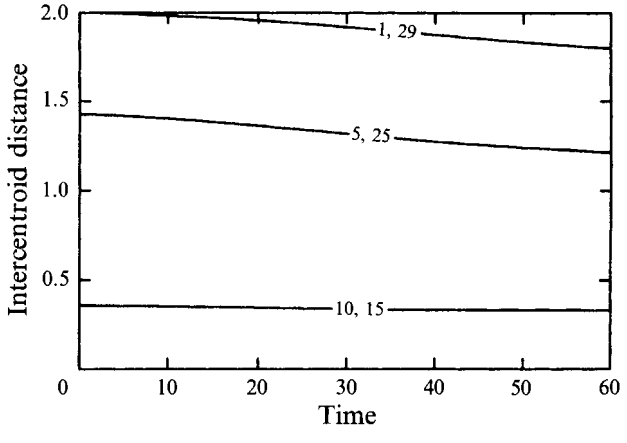

FIGURE 18. The intercentroid distances for $\gamma/V_h = 3$ (Run 4).

28, 29 show signs of steepening at $t = 60$. The inner levels 5 and 25 retain a rounded oval shape up to the end of the run. The extent of wobbling has also been reduced as shown by the trajectories of the centroids of levels 1 and 29 in figure 17. The paths are nearly circular arcs of short length and do not spiral inwards as do the trajectories in

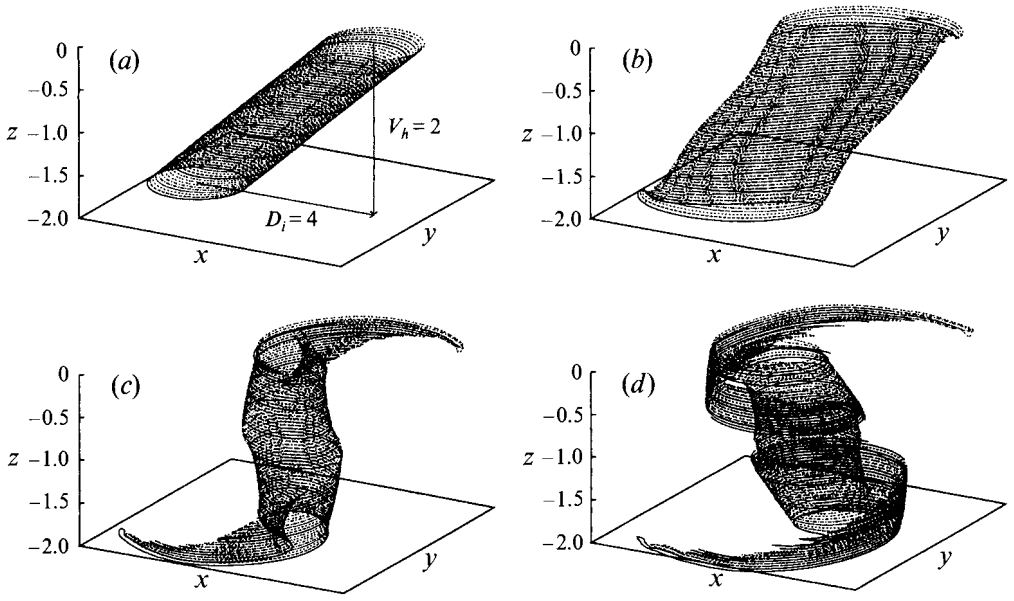

FIGURE 19. The vortex evolution for $D_i/V_h = 2$ and $\gamma/V_h = 0.5$. Here $N_z = 61$ and $\Delta z = 0.0333$ (Run 5): (*a*) $t = 0$, (*b*) $t = 20$, (*c*) $t = 40$, (*d*) $t = 60$.

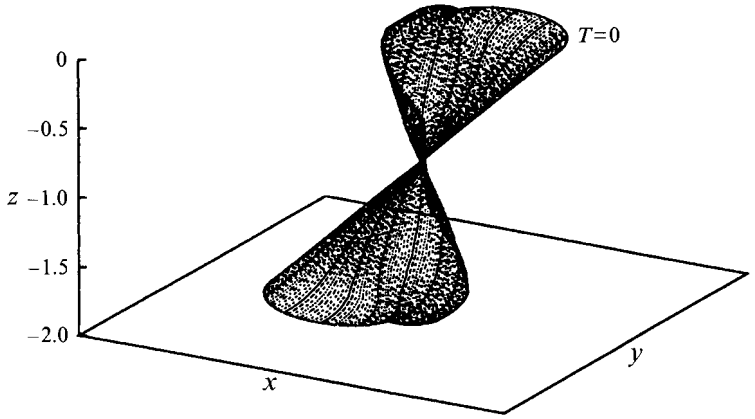

FIGURE 20. Evolution of the vortex axis for $\gamma/V_h = 0.5$ (Run 5).

figures 3 and 13. This means that alignment of the outer levels has been considerably suppressed, as confirmed by the intercentroid distance plots in figure 18. All curves have an almost constant slow rate of decay, with $d_c(10, 15)$ remaining virtually constant throughout the evolution. The fractional decrease of the alignment curve $d_c(1, 29)$ is only $\Delta D \approx 10\%$ at $t = 60$.

In the last simulation (Run 5), we decrease the effective stratification strength to $\gamma/V_h = 0.5$ by increasing the vortex height to $V_h = 2$ and letting $\gamma = 1$. We set $D_i = 4$ and hence the angle of tilt is unchanged with $\tan\theta_i = 2$. The number of vertical points is increased to $N_z = 61$ to maintain an adequate resolution. The three-dimensional plots in figure 19 show that the main effect of the weaker stratification is to accelerate the evolution and thereby increase the extent of filamentation in the top and bottom parts of the vortex. This, in turn, increases the tendency of vertical alignment and horizontal axisymmetrization. There is a visible vertical distortion of the vortex at $t = 40$ and it

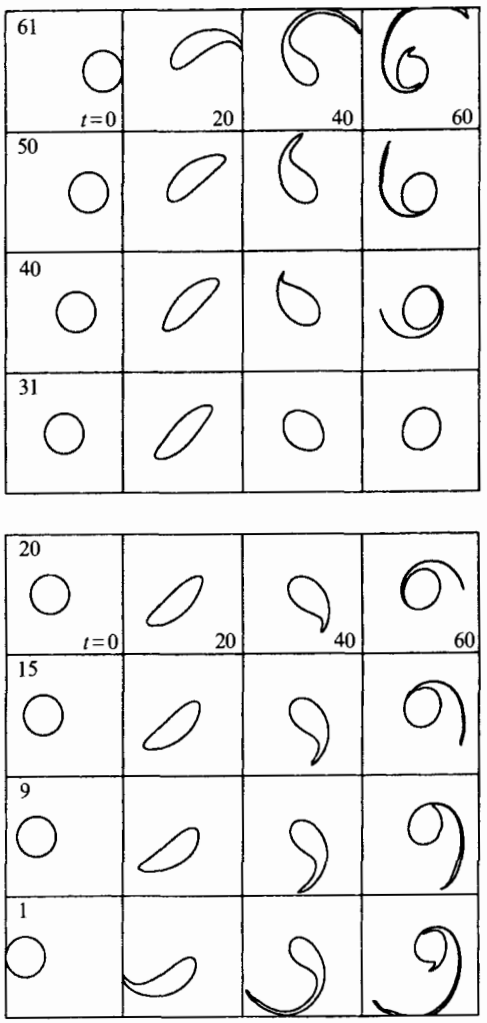

FIGURE 21. Evolution of the horizontal cross-sections for $\gamma/V_h = 0.5$ (Run 5).

becomes more pronounced at $t = 60$. The evolution of the vortex axis in figure 20 clearly shows the extent of vertical distortion experienced by the vortex at the end of the run.

The evolution of the horizontal cross-sections is shown in figure 21. Note, in particular, the elongated shape of the boundaries at $t = 20$, which resemble the elongated shapes at $t = 20$ of the case $D_i/V_h = 4$ of figure 6. At $t = 40$ however, the centre level 31 returns to a more rounded configuration compared to the highly distorted shape of the corresponding middle level 15 of figure 7. Finally, at $t = 60$ all levels reach a high degree of axisymmetry and in particular level 31 becomes almost circular without filamentation. The outer levels 1–9 and 50–61 have long and wide filamentary tails which are about to detach from the vortex core. The bottom and top levels 1 and 61 show further steepening of the boundary which may conceivably lead to further breaking and filamentation. The paths of the centroids of the top and bottom levels 1 and 61 (figure 22), have the shape of long arcs of low curvature, except near the end of the run where there is a sudden change of curvature. The relatively small distance between the end points of the paths shows the large tendency towards vertical

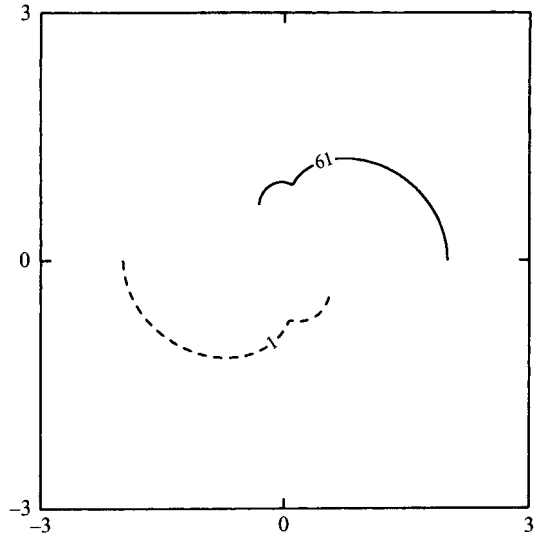

FIGURE 22. Trajectories of the centroids of levels 1 and 61 for $\gamma/V_h = 0.5$ (Run 5).

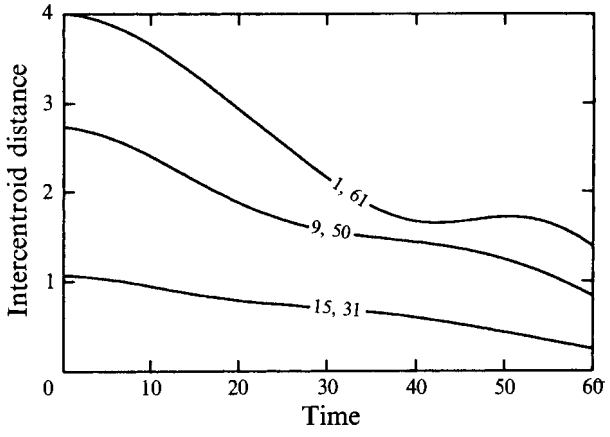

FIGURE 23. The intercentroid distances for $\gamma/V_h = 0.5$ (Run 5).

alignment. The intercentroid distances in figure 23 confirm the large degree of alignment. The curve $d_c(1, 61)$ decays to a value $D_f \approx 1.4$ from the initial value $D_i = 4$, giving a fractional decrease of $\Delta D \approx 65\%$ at $t = 60$. This should be compared with the value $\Delta D \approx 50\%$ obtained in Run 1. The curves $d_c(9, 50)$ and $d_c(15, 31)$ also decrease quite considerably, with the former reaching a fractional decrease $\Delta D \approx 68\%$ at the end of the evolution.

We now give a quantitative measure of the amount of potential vorticity and enstrophy of the vortex in Run 5 that moves from the circularizing core into the filaments. In figure 24 we plot the fractional area of the detaching filaments in the lower half of the vortex, as a function of z. The fractional area is calculated as A_F/A_T, where A_F is the filament area and A_T is the total area of the horizontal cross-section at the given value of z. The bottom level at $z = -2$ transfers 30% of its area to filamentation. The filament area decays to zero within a distance of about 0.6 (at $z \approx -1.4$), which corresponds to about 30% of the total vortex height. We note that the area under the

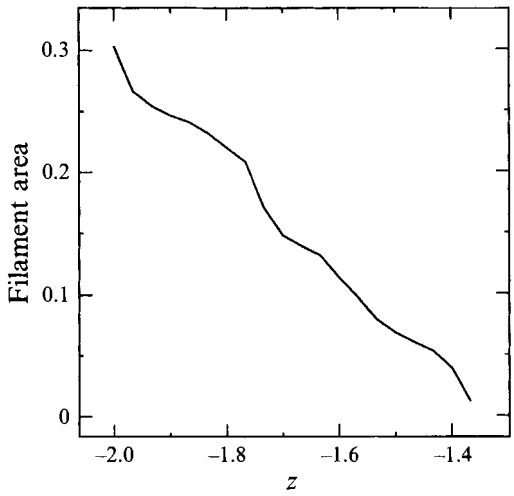

FIGURE 24. The fractional area of the detached filaments of the vortex of Run 5, as a function of z. The curve represents the area of the filaments at $t = 60$ in figure 21, expressed as a fraction of the total cross-sectional area of the vortex as a given value of z. Only the area corresponding to the lower half of the vortex is shown. The area under the curve multiplied by 2 gives the total fractional volume of vortical fluid lost to filamentation.

curve in figure 24 (i.e. the integral with respect to z from -2 to -1.4), gives the fractional volume lost to filamentation in the lower half. Multiplying by 2 to include the volume lost in the upper-half as well gives a total volume lost of $\Delta V_F \approx 0.18$. Hence, 18% of the total vortex volume of 2π is lost effectively irreversibly by filamentation. Since the potential vorticity is uniform, both horizontally and vertically, the potential enstrophy V, defined as the volume average of $\frac{1}{2}Q^2$, is proportional to the volume lost. Therefore the curve in figure 24 also gives the variation of the potential enstrophy with z and a measure of the total amount that moves away from the vortex core due to the filamentation process.

4. Summary and discussion

We have analysed the evolution of a vertically tilted geostrophic vortex using the Lagrangian method of boundary surface dynamics. We used a simple cylindrical vortex of circular horizontal cross-section, consisting of a finite volume of constant potential vorticity embedded in a spatially unbounded continuously stratified fluid of uniform Brunt–Väisälä profile. The numerical experiments show that the vortex wobbles about its centre and its boundary surface steepens and filaments in order to achieve a vertically aligned axisymmetrical configuration. As discussed by McWilliams (1989), we found it convenient to make a distinction between two separate stages of the evolution. First, the initially circular horizontal cross-sections distort and elongate to allow vertical alignment of the centroids of the different sections to occur. Secondly, the distorted horizontal sections axisymmetrize, often but not always, through the process of filamentation. It is the combination of these processes that eventually leads to the final vertically aligned axisymmetrical shape. Depending on the parameter values of the model, the vortex achieves various degrees of vertical alignment and horizontal axisymmetry within the time interval used in the present simulations, but never reaches a perfect upright position with circular horizontal cross-sections.

However, we have been able to identify general conditions that enhance or suppress the two process in a volume of fluid with a single sign in the vorticity field as is relevant to the study of turbulent flows.

We have also been able to partially answer some of the questions raised in §1 regarding the interaction of two vertically offset vortices. For example, the tilted vortex appeared to be stable and align under most conditions, at least for the parameter values used in the present simulations. In particular, the simulations also show that increasing the tilt angle up to a certain extent has the effect of increasing the rate of vertical alignment of the top and bottom sections, at least in the early stages of the evolution. For instance, the rate of decay, from $t = 0$ to the first minimum, of the intercentroid distance curve $d_c(1, 29)$ in figure 10 (Run 2), is almost twice as large as for the same curve in figure 5 (Run 1). What happens when the tilt angle is increased even further remains an open question to be answered through more numerical experimentation. It was also found that for relatively small inclination angles, only the sections near the top and bottom levels of the vortex break and filament. However, increasing the tilting angle has the effect of increasing the horizontal distortion and steepening on all sections of the vortex surface. This leads not only to an increase in the length and width of the filaments ejected in the upper and lower sections, but also to steepening and breaking with consequent filamentation in the middle levels of the structure. This is clearly seen by comparing figures 1 and 6 at $t = 60$.

We also ran simulations for varying stratification strength γ/V_h and found that, for a fixed vortex height, if the horizontal scale of the flow is less than the internal radius of deformation L_D, the degree of vertical alignment, filamentation, and axisymmetrization is greatly inhibited. Studies of the evolution of a right elliptical cylinder vortex by Viera (1994*b*) showed a similar behaviour in which axisymmetrization and filamentation were both suppressed when L was less than L_D. This dependence of the numerical experiments on the deformation radius is consistent with the usual relationship of the ratio of potential energy (PE) to kinetic energy (KE). That is, accelerated alignment and axisymmetrization (barotropization) occurs with greater PE/KE ratio, or equivalently, with greater horizontal scale relative to the deformation radius.

We also calculated the potential vorticity and enstrophy that is lost irreversibly from the circularizing core to the filaments of the vortex in Run 5. Since in this case the filaments have a larger area compared with the filaments found at the end of the other simulations (cf. figures 4, 7, 12 and 15), it provides an upper bound for the amount of potential vorticity that is lost for all the evolutions presented here. The filament area decays rapidly with z as we approach the vortex centre, and is confined to the top 30% and bottom 30% of the vortex surface. We should point out that the presence of horizontal boundaries may affect the potential vorticity lost to filamentation near the top and bottom sections of the vortex. In fact, recent preliminary simulations with one horizontal boundary present (not yet published) seem to indicate that horizontal axisymmetrization is enhanced near the boundary and at the same time the amount of filamentation is reduced. More numerical experiments are required to confirm these findings.

In order to minimize the number of parameters involved, we have assumed a simple vortex of constant potential vorticity distribution. In the real oceans and atmosphere, however, the potential vorticity varies in both the horizontal and vertical directions. Simulations with more realistic variations than those used here would be desirable, to model actual physical situations more accurately. While arbitrary variations of potential vorticity in the vertical direction are relatively simple to implement using

BSD (see (4)), variations in the horizontal direction would require a formulation involving a multi-surface piecewise-constant distribution to approximate a continuous potential vorticity distribution. This is not difficult to implement, but would increase the computational time required for each simulation quite considerably. Finally, we would like to emphasize that the vortex considered here consisted of a simple cylinder of linear axis and circular horizontal cross-section at $t = 0$. For the purpose of understanding in more detail the process of emergence of coherent vortices from random initial distributions of potential vorticity, it would be highly relevant to study the simultaneous effects of (*a*) vertical tilting, (*b*) initially distorted (perhaps near elliptical) horizontal cross-sections and (*c*) a vortex axis that initially departs from the linear shape. These generalizations would increase the number of model parameters available. More numerical experiments would therefore be necessary to fully understand the nature of the alignment and axisymmetrization processes in a continuously stratified, quasi-geostrophic fluid.

I would like to thank two anonymous reviewers, whose comments and positive criticisms greatly helped to improve the presentation of this paper.

REFERENCES

CHARNEY, J. G. 1963 Numerical experiment in atmospheric hydrodynamics. *Proc. Symp. Appl. Math., Am. Math. Soc.* **15**, 289–310.

MCWILLIAMS, J. C. 1984 The emergence of isolated coherent vortices in turbulent flow. *J. Fluid Mech.* **146**, 21–43.

MCWILLIAMS, J. C. 1989 Statistical properties of decaying geostrophic turbulence. *J. Fluid Mech.* **198**, 199–230.

MCWILLIAMS, J. C. 1990 The vortices of two-dimensional turbulence. *J. Fluid Mech.* **219**, 361–385.

MELANDER, M. V., MCWILLIAMS, J. C. & ZABUSKY, N. J. 1987 Axisymmetrization and vorticity-gradient intensification of an isolated two-dimensional vortex through filamentation. *J. Fluid Mech.* **178**, 137–159.

MELANDER, M. V., ZABUSKY, N. J. & MCWILLIAMS, J. C. 1988 Symmetric vortex merger in two dimensions: causes and conditions. *J. Fluid mech.* **195**, 303–340.

PEDLOSKY, J. 1979 *Geophysical Fluid Dynamics*, chap. 6. Springer.

POLVANI, L. M. 1991 Two-layer geostrophic dynamics. Part 2. Alignment and two-layer V-states. *J. Fluid Mech.* **225**, 241–270.

POLVANI, L. M., ZABUSKY, N. J. & FLIERL, G. R. 1989 Two-layer geostrophic dynamics. Part 1. Upper-layer V-states and merger. *J. Fluid Mech.* **205**, 215–242.

RHINES, P. B. 1977 The dynamics of unsteady currents. In *The Sea*, vol. 6, pp. 189–318. Wiley.

RHINES, P. B. 1979 Geostrophic Turbulence. *Ann. Rev. Fluid Mech.* **11**, 401–441.

VIERA, F. 1994*a* Boundary Surface Dynamics: An algorithm for stratified geostrophic flows. *J. Comput. Phys.* **111**, 336–346.

VIERA, F. 1994*b* The evolution of cylindrical geostrophic vortices. *Proceedings: Computational Techniques and Applications: CTAC-93*, pp. 462–469. World Scientific.

VIERA, F. 1994*c* The dynamics of stratified geostrophic vortices. Part 1. Combined merger/alignment simulations. *Res. Rep.* 94-12. School of Mathematics and Statistics, The University of Sydney.